NANO LETTERS

Letter

pubs.acs.org/NanoLett

Nanopillar Spin Filter Tunnel Junctions with Manganite Barriers

Bhagwati Prasad,*[,†] Mehmet Egilmez,[†,§] Frank Schoofs,[†] Thomas Fix,[†,∥] Mary E. Vickers,[†] Wenrui Zhang,[‡] Jie Jian,[‡] Haiyan Wang,[‡] and Mark G. Blamire[†]

[†]Department of Materials Science and Metallurgy, University of Cambridge, 27 Charles Babbage Road, Cambridge, CB3 0FS, U.K.

[‡]Department of Electrical and Computer Engineering, Texas A&M University, College Station, Texas 77843-3128, United States

Supporting Information

ABSTRACT: The potential of a manganite ferromagnetic insulator in the field of spin-filtering has been demonstrated. For this, an ultrathin film of $Sm_{0.75}Sr_{0.25}MnO_3$ is integrated as a barrier in an epitaxial oxide nanopillar tunnel junction and a high spin polarization of up to 75% at 5 K has been achieved. A large zero-bias anomaly observed in the dynamic conductance at low temperatures is explained in terms of the Kondo scattering model. In addition, a decrease in spin polarization at low bias and hysteretic magneto-resistance at low temperatures are reported. The results open up new possibilities for spin-electronics and suggest exploration of other manganites-based materials for the room temperature spin-filter applications.

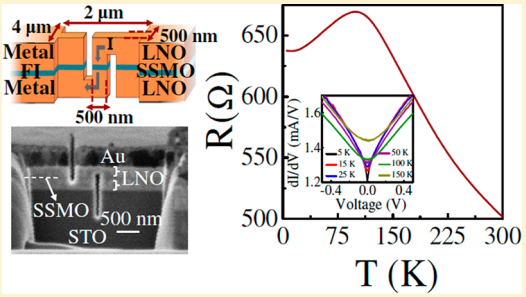

KEYWORDS: *Spin filter, nanopillar, tunnel barrier, manganites, Kondo effect*

In the last two decades, the development of nanostructured electronic devices has benefited from the use of the carriers' spin degree of freedom. This has led to many potential applications such as nonvolatile magnetic memories, reprogrammable logic and quantum computers.[1,2] These devices rely on the generation of highly spin-polarized currents. Spin filter tunnel junction (SFTJ) has emerged as a promising alternative for this purpose. A possible way is to sandwich a few-nanometer thin ferromagnetic insulator (FI) film between the metallic electrodes and generate a highly spin-polarized current by preferential tunneling of electrons in one spin direction.[3] This happens because of exchange splitting of the FI conduction band, which, in turn, lowers the barrier height for the electrons of one of the two spin directions. Since the tunneling probability increases exponentially with the reduction of barrier height, a SFTJ can effectively produce almost a fully spin-polarized current.

Spin-filtering effects have been studied extensively in ferromagnetic insulating europium chalcogenides[4−6] and GdN[7,8] tunnel barriers. However, low Curie temperatures (T_C) and poor chemical compatibility with potential electrodes limit their application in spin filtering. FI ferrites such as $NiFe_2O_4$, $CoFe_2O_4$, and $MnFe_2O_4$ are alternatives with a much higher T_C,[9−11] and Matzen et al.[12] have reported the highest spin-polarization (−8%) value at room temperature with a $CoFe_2O_4$ based spin-filter. Nevertheless the complex crystal structures of ferrites make their integration as tunnel barriers in SFTJ devices challenging. A topical solution lies with the use of perovskite-type manganites. They are routinely grown as thin films as well as lattice-matched epitaxial heterostructures. Another advantage being their chemical and structural compatibility with numerous oxide electrodes.[13] In particular, manganites have been widely explored as electrodes in magnetic tunnel junctions (MTJ).[14] Their application as a FI tunnel barriers (in SFTJs), is now emerging. One recent example is provided by Harada et al.[15] with a $Pr_{0.8}Ca_{0.2}Mn_{1-y}Co_yO_3$ tunnel barrier. Among the wide panel of manganite systems, $Sm_{1-x}Sr_xMnO_3$ offers several key advantages. It exhibits a well-defined ferromagnetic insulating phase for the composition $0.1 \leq x \leq 0.3$ below its Curie temperature (~100 K),[16,17] good lattice matching with conductive oxide electrodes such as $LaNiO_3$ (LNO), etc. This enables the challenging concomitant tuning of ferromagnetic properties and structural integration into devices. At low temperature (below T_C), bulk $Sm_{1-x}Sr_xMnO_3$ ($0.1 \leq x \leq 0.3$) is a phase-separated magnetic system, consisting of a mixture of a dominant ferromagnetic (FM) and an antiferromagnetic (AF) phases. Despite negligible contribution of the AF phase on the magnetic properties, transport measurements reveal an insulating behavior without colossal magnetoresistance effects.[17] Therefore, $Sm_{1-x}Sr_xMnO_3$ ($0.1 \leq x \leq 0.3$) is classified as a promising FI tunnel barrier material for SFTJ.

In this work, we investigate the spin filtering properties of $Sm_{0.75}Sr_{0.25}MnO_3$ (SSMO) manganite ultrathin films in LNO/SSMO/LNO tunnel junctions. SSMO films were grown by pulsed laser deposition (PLD) onto $SrTiO_3$ (001) substrates in an N_2O atmosphere (for details, see the Experimental Section). The XRD pattern ($2\theta-\omega$ scan) and the Φ scan of the (111) reflection of an 18 nm thick SSMO film depicted in Figure 1a,b confirm the epitaxial growth with 45° in-plane rotation vis-à-vis

Received: March 2, 2014
Revised: April 15, 2014
Published: April 17, 2014

   dx.doi.org/10.1021/nl500798b | *Nano Lett.* 2014, 14, 2789−2793

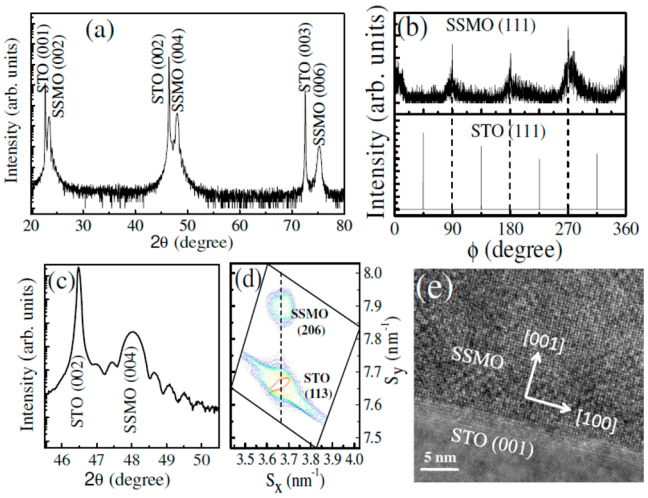

Figure 1. (a) X-ray diffraction pattern ($2\theta-\omega$ scan) of an 18 nm thick SSMO film on STO (001). (b) Φ scan around the (111) reflection of SSMO (top) and STO (bottom). (c) Diffraction fringes in the vicinity of the (004) reflection of SSMO. (d) RSM around the (206) reflection of SSMO along with the (113) reflection of STO. The vertical line joining the SSMO and STO reflections indicates that the film is fully strained in-plane. (e) Cross-sectional HRTEM image of a SSMO film deposited on STO (001).

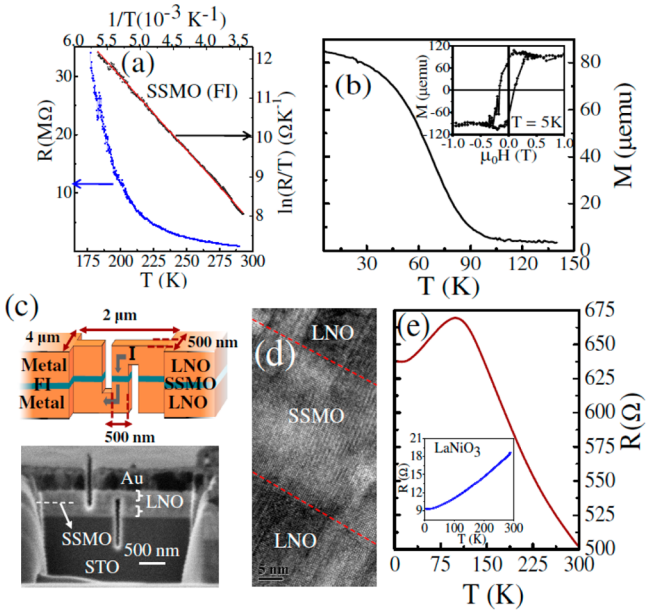

Figure 2. (a) Resistance as a function of temperature of an 18 nm thick SSMO film and the corresponding variable range hopping plot (black dots) with a least-squares linear fit (in red). (b) Magnetization versus temperature plot for a LNO/SSMO (5 nm)/LNO trilayer sample measured in a magnetic field corresponding to 0.1 T. Inset shows magnetization hysteresis loop for the sample at 5 K after subtracting the paramagnetic contribution from LNO layers. The magnetic field is applied in plane to the sample. (c) Schematic diagram and cross section image (SEM) of the nanopillar tunnel device. (d) Cross-sectional TEM image of a LNO/SSMO(30 nm)/LNO trilayer sample. (e) Temperature dependence of the junction resistance of a Au/LNO/SSMO(5 nm)/LNO tunnel junction measured at a current of 1 mA. The inset shows the $R-T$ plot for a LNO single film.

the substrate, i.e. the alignment of [110] of orthorhombic SSMO with the [100] of the underlying cubic $SrTiO_3$ (STO) substrate. Film thickness was calculated from both X-ray reflectivity (not shown) and diffraction fringes around the (004) reflection of SSMO (Figure 1c). The full width at half-maximum (fwhm) values of the rocking curves for (004) reflection of the film and that (002) of the substrate were found to be the same (0.04°), demonstrating thereby a high degree of crystalline orientation of the film. Figure 1d shows the reciprocal space map (RSM) around the (206) reflection of the film along with the (113) reflection of the substrate, which indicates that the film is fully strained in-plane. Epitaxial growth and high crystallinity are further confirmed by transmission electron microscopy (TEM) of a SSMO film deposited on a STO (001) substrate under the same growth condition (Figure 1e). The uniformity of the image contrast in the film area suggests that the composition is homogeneous. The cationic composition of the film was investigated from the energy dispersive spectroscopy analysis on a duplicate film grown on an $NdGaO_3$ (001) substrate in the same run, and found to be in excellent agreement with that of the target.

The resistance versus temperature plot (Figure 2a) of an 18 nm thick SSMO film indicates its insulating nature below room temperature. Resistance of the film increased beyond the measurement limit below 175 K. The electrical transport mechanism of the film at higher temperatures (i.e., under paramagnetic regime) can be explained by the Emin-Holstein[18,19] small polaron hopping (SPH) model in the adiabatic limit. Accordingly, the resistance $R(T)$ is given by

$$R(T) = AT \exp\left(\frac{E_A}{k_B T}\right) \quad (1)$$

where E_A is the activation energy, T is the temperature, and A is a constant determined by polaron concentration and hopping length. In manganites, the strong electron−phonon interaction leads to the formation of such small polarons.[20] The value of E_A obtained by least-squares linear fitting of $\ln(R/T)$ versus $1/T$ plot is 160 meV, higher than the 45−56 meV of the corresponding bulk.[21] This amounts to reduction in charge transport and can be attributed to epitaxial strains and impending structural distortions in the epitaxial film.

In order to demonstrate the tunnel barrier potential of SSMO in a SFTJ, a trilayer structure of LNO(200 nm)/SSMO(5 nm)/LNO(200 nm) was grown epitaxially on STO (001) substrate. The temperature dependence of magnetization of this trilayer structure reveals occurrence of a ferromagnetic transition around 100 K (Figure 2b), just as one observes in a freestanding SSMO film (not shown). The magnetic hysteresis loop is included in the inset of Figure 2b after subtracting the paramagnetic contribution of LNO layers. The paramagnetic nature of LNO thin films (200 and 400 nm) was verified earlier. The lattice matched epitaxial growth of SSMO film on LNO electrode (200 nm film) was confirmed by XRD measurements (see Supporting Information). The trilayer system was then fabricated to obtain nanopillar tunnel junctions of area around 500 × 500 nm^2 (Figure 2c). The quality of the interfaces between the electrode and the barrier layers was explored by the cross sectional TEM study where a 30 nm thick SSMO film is sandwiched between the two LNO layers (Figure 2d). The interfaces do not seem well defined and so spin-disorder clusters of SSMO might exist there. The temperature dependent junction resistance of the Au/LNO/SSMO(5 nm)/LNO device at higher temperatures (Figure 2e) shows a typical characteristic of a semiconducting barrier (i.e., the

dx.doi.org/10.1021/nl500798b | Nano Lett. 2014, 14, 2789−2793

junction resistance increases with decreasing T below room temperature), whereas at low temperatures (below ~ 100 K) the junction resistance decreases. In contrast, a freestanding LNO thin film shows a metallic behavior, i.e., monotonic decrease in resistance upon cooling (inset of Figure 2e). With insulating-like SSMO film and the metallic LNO, the semiconducting-like temperature dependence of the junction resistance at high temperatures suggest occurrence of electron tunneling through the barrier. As the device is cooled below the ferromagnetic transition temperature (T_C ~ 100 K) of SSMO layer, the junction resistance decreases due to the lowering of the tunnel barrier height for spin-up electrons caused by the exchange splitting. On the contrary, resistance increases monotonically with decreasing temperature in a nonmagnetic tunnel junction.[22] Indeed, decrease of junction resistance below the ferromagnetic transition temperature here provides a clear evidence of spin filtering through SSMO film, as in other SFTJs.[5,7,23]

Figure 3a shows the dynamic conductance versus voltage plots of the tunnel junction at various temperatures. The nearly

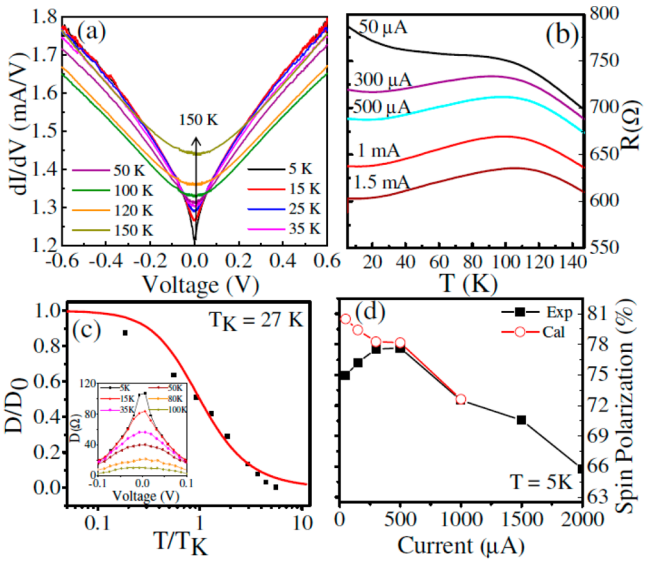

Figure 3. (a) Dynamic conductance versus voltage plots for a Au/LNO/SSMO (5 nm)/LNO tunnel junction at various temperatures. (b) Resistance as a function of temperature of the tunnel junction with varying current bias. (c) Normalized excess dynamic resistance at zero bias vs. T/T_k. The solid line is a fit with the empirical formula given in Equation (2). Inset shows the excess dynamic resistance at lower bias with varying temperature emphasizing the contribution of the additional scattering process. (d) Variation of the spin polarization of the junction at 5 K with applied bias (experimental in black and calculated in red by subtracting the additional scattering process visible at lower bias).

parabolic shape of the dynamic conductance curve at higher temperatures reveals that the dominating mode of electron transport through the junction is tunneling. The barrier height of the tunnel junction is determined by fitting the current−voltage (I−V) curve to Simmons model[24] above T_C (see Supporting Information). The average barrier height thus obtained is 0.5 eV, which is typical band gap for the perovskite manganites.[25] At lower temperatures, the dynamic conductance curve exhibits a zero bias anomaly (ZBA), suggesting operation of additional scattering processes at low bias. This ZBA diminishes slowly with increasing temperature.

Small zero-bias anomaly observed earlier in SFTJs,[26,27] has been explained in terms of electron tunneling assisted by magnon or phonon excitations (i.e., inelastic scattering). However, large ZBA found in SFTJ here suggests role of a different scattering mechanism, possibly involving impurities present at the interface. The impurities may act as scattering centers for tunneling electrons modifying thereby the interfacial density of states.[28,29] Several attempts have been made to understand the mechanism of interface impurity assisted electron transport through the barrier.[30−32] For the magnetic impurities induced large ZBA peaks in dynamic resistance in tunnel junctions are explained by the Kondo scattering model.[33−35]

In addition to ZBA, the R versus T plots of the spin filter tunnel device at different currents (Figure 3b) show decrease in extent of resistance drop below the magnetic transition temperature with decreasing current. It means that the device resistance is higher than a SFTJ at a lower current due to the additional scattering becoming active at low temperatures. However, at high currents (1 and 1.5 mA), R−T plots follow the expected trend. In order to investigate the contribution of various scattering processes to electron transport across the junction, the additional dynamic resistance at lower currents (denoted by D) is calculated (inset of Figure 3c). For this, the dynamic resistance without any scattering process obtained from the fitted I−V data to Simmons model at different temperatures is subtracted from the corresponding experimental value. The temperature dependence of D at zero-bias is plotted in Figure 3c with two scaling parameters D_0 and T_K. Here D_0 is the extrapolated value of D at T = 0 K and T_K is the temperature at which $D(T_K) = D_0/2$. The solid line represents the fitted data with the following empirical relation[36] for the fitting parameter (s) = 0.738.

$$\frac{D}{D_0} = \left[1 + (2^{1/s} - 1)\left(\frac{T}{T_K}\right)^2\right]^{-s} \quad (2)$$

The logarithmic dependence of D on T and the scaling behavior give signature of Kondo-like effect in the fabricated SFTJ; the Kondo temperature (T_K) being around 27 K. Lee et al.[35] have also observed large ZBA in magnetic tunnel junctions and explained by Kondo effect arising due to presence of magnetic impurities at the interface. In the present SFTJ, coexistence of ferromagnetic, spin glass and/or antiferromagnetic clusters at the barrier-electrode interfaces is possible because the interface is not abrupt (as revealed by cross-sectional TEM image, Figure 2d). These spin-disorder and/or antiferromagnetic clusters perhaps act as scattering centers for tunneling electrons, producing thereby the Kondo-like effect. A small amount of spin-disordered clusters in a ferromagnetic phase is reported to trigger a Kondo-like behavior at low temperatures.[37] Figure 3d shows the effective spin polarization as a function of applied bias with and without considering the Kondo effect. The spin filtering efficiency of the junction can be calculated by the method given elsewhere (see Supporting Information).[7,8] Our SFTJ exhibits a spin-polarization up to 75% at 5 K, which is nearly double to reported oxide based junction.[15] Reduction in spin filtering efficiency at lower bias can be correlated with Kondo scattering at low temperature.

Figure 4a shows sharp decrease in junction resistance (with 500 μA current at 5 K) with increase in magnetic field. On reversing the direction of the magnetic field the resistance increases again but the virgin curve is never recovered. When

dx.doi.org/10.1021/nl500798b | Nano Lett. 2014, 14, 2789−2793

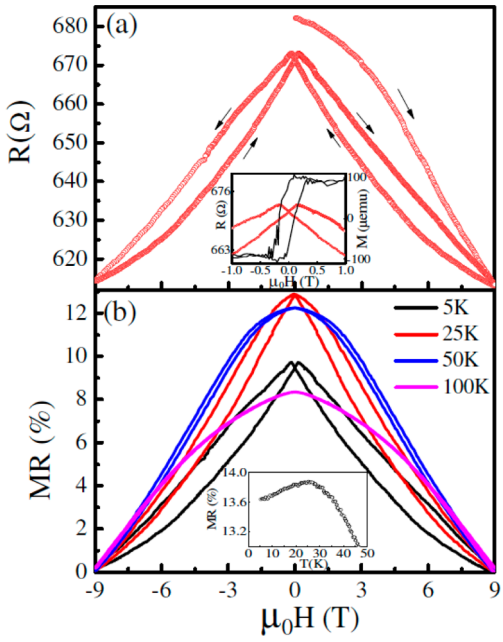

Figure 4. (a) Junction resistance as a function of in-plane applied magnetic field at 5 K of a zero field cooled tunnel device measured with a current of 500 μA. Inset depicts that the peak of the $R-H$ curve coincides with the coercive field of SSMO. (b) Isothermal magnetoresistance (MR) of the tunnel device at 5, 25, 50, and 100 K. Inset shows the temperature dependence MR of the device.

decreasing from + 9T, a peak of the resistance appears at −0.2 T, which is the coercive field of SSMO (inset of Figure 4a). With the subsequent cycles of the magnetic field, the resistance of the device shows hysteresis. This can be explained by the coexistence of AF with FM phases in SSMO. Upon applying a magnetic field, a fraction of the AF phase transforms to FM and the SSMO barrier layer exhibits a metamagnetic transition.[38] As a consequence, the net ferromagnetism of the barrier layer is enhanced, which increases the exchange splitting and causes reduction in the barrier height for the tunneling of spin-up electrons. Similar field dependent exchange splitting has been observed in the case of EuSe barrier.[5] Note that the EuSe is an antiferromagnet but becomes ferromagnetic with a small applied magnetic field. The isothermal magnetoresistance (MR), $\Delta R/R(\mu_0 H$ = 9 T), plots of the device are shown in Figure 4b. At low temperatures, the MR curve shows hysteresis upon sweeping the magnetic field, which points toward the occurrence of a first order phase transition in the barrier layer.[39] With increasing magnetic field, the spins can be aligned easily but more energy is required for their rotation under the reverse field. The hysteretic nature of the MR curve reduces with increasing temperature and completely diminishes at 100 K. The temperature dependence of the device MR at 500 μA is shown in the inset of Figure 4b. It first increases with decrease in temperature below100 K and then begins to decrease at some point. This is at variance with the temperature dependence magnetization behavior of SSMO. The decrease in MR below 27 K can be understood by the Kondo scattering of the spin-polarized electrons. Nevertheless, a more complete understanding of the physical properties of SSMO is required to fully understand the details of the tunneling mechanisms in these SFTJs.

To conclude, the spin filtering nature of an ultrathin $Sm_{0.75}Sr_{0.25}MnO_3$ manganite film in a tunnel junction has been realized. It shows spin polarization of as high as 75% at 5K. The large zero-bias anomalies in dynamic conductance at low temperatures can be understood in terms of the Kondo scattering model. Below the T_C of SSMO, the lowering of the junction resistance with increase in magnetic field and the hysteretic nature of magnetoresistance arise due to a soft metamagnetic transition occurring in the barrier layer. The work paves way for the development of novel spin-filter devices and is likely to stimulate further research on manganites-based tunnel junctions.

Experimental Section. SSMO and LNO thin films were grown by PLD on STO (001) (Crystal GmbH) substrates using stoichiometric $Sm_{0.75}Sr_{0.25}MnO_3$ and $LaNiO_3$ targets prepared by a standard solid-state reaction method from high purity powders in the appropriate proportions. A Lambda Physik KrF excimer laser (λ = 248 nm) was used at 5 Hz repetition rate. The laser energy density was set at ∼1 J/cm^2 on the target with a target-to-substrate distance of 4 cm. The optimized substrate temperature and N_2O gas pressure for the deposition of SSMO (and LNO) films were 700 °C (and 650 °C) and 20 Pa (and 30 Pa), respectively. After growth, films were cooled down to room temperature in 100 Pa N_2O. A PANalytical high resolution X-ray diffractometer (with Cu K_α radiation, a 2-bounce hybrid monochromator and 0.5 mm slit beam tunnel) was used to determine the phase and crystalline quality of the deposited films. Epitaxial LNO/SSMO/LNO trilayer structures were deposited on atomically flat STO (001) substrates at the optimized deposition conditions. The thickness of both top and bottom LNO layers was ∼ 200 nm. Polycrystalline gold layer was deposited by standard DC magnetron sputtering to serve as a top contact. A series of 4 μm tracks were first patterned by optical lithography and then created with argon-ion milling. Finally, the nanopillar devices with an average dimension of 500 nm × 500 nm were fabricated using focused ion beam (FIB) nanomachining technique described elsewhere.[40,41] Transport measurements were carried out in four-point configuration in a closed-cycle He cryostat system.

■ ASSOCIATED CONTENT

Supporting Information

Additional XRD, Simmons fitting of the $I-V$ curve, AFM image, and a method for calculating spin polarization. This material is available free of charge via the Internet at http://pubs.acs.org.

■ AUTHOR INFORMATION

Corresponding Author

*(B.P.) E-mail: bp337@cam.ac.uk.

Present Addresses

[§]Department of Physics, American University of Sharjah, PO Box 26666, Sharjah, UAE

[‖]ICube laboratory (Université de Strasbourg and CNRS), 23 rue du Loess BP 20 CR, 67037 Strasbourg Cedex 2, France

Author Contributions

B.P. is responsible for the experiments and preparation of the paper; FS. and M.E.V. contributed to XRD work; M. E. contributed to the device fabrication; W.Z., J.J., and H.W. performed the TEM analysis; F.S, T.F., and M.G.B. provided guidance for the experiments and for editing and proofreading the paper.

Notes

The authors declare no competing financial interest.

■ ACKNOWLEDGMENTS

This work was partially supported by the ERC Advanced Integrators Grant "SUPERSPIN". B.P. was funded by the Nehru Trust for Cambridge University and St John's College. The TEM work at Texas A&M was supported by the U.S. National Science Foundation (NSF-DMR 0846504). The authors wish to thank Prof. J. Kumar (IIT Kanpur, India) for help in improving the manuscript.

■ REFERENCES

(1) Prinz, G. A. *Science* **1998**, *282*, 1660.
(2) DiVincenzo, D. P. *Science* **1995**, *270*, 255.
(3) Moodera, J. S.; Santos, T. S.; Nagahama, T. *J. Phys: Condens. Matter* **2007**, *19*, 165202.
(4) Moodera, J. S.; Hao, X.; Gibson, G. A.; Meservey, R. *Phys. Rev. Lett.* **1988**, *61*, 637.
(5) Moodera, J. S.; Meservey, R.; Hao, X. *Phys. Rev. Lett.* **1993**, *70*, 853.
(6) Santos, T. S.; Moodera, J. S. *Phys. Rev. B* **2004**, *69*, 241203(R).
(7) Pal, A.; Senapati, K.; Barber, Z. H.; Blamire, M. G. *Adv. Mater.* **2013**, *25*, 5581.
(8) Senapati, K.; Blamire, M. G.; Barber, Z. H. *Nat. Mater.* **2011**, *10*, 849.
(9) Lüders, U.; Barthélémy, A.; Bibes, M.; Bouzehouane, K.; Fusil, S.; Jacquet, E.; Contour, J. -P.; Bobo, J. -F.; Fontcuberta, J.; Fert, A. *Adv. Mater.* **2006**, *18*, 1733.
(10) Chapline, M. G.; Wang, S. X. *Phys. Rev. B* **2006**, *74*, 014418.
(11) Matzen, S.; Moussy, J. -B.; Miao, G. X.; Moodera, J. S. *Phys. Rev. B* **2013**, *87*, 184422.
(12) Matzen, S.; Moussy, J.- B.; Mattana, R.; Bouzehouane, K.; Deranlot, C.; Petroff, F. *Appl. Phys. Lett.* **2012**, *101*, 042409.
(13) Haghiri-Gosnet, A. -M.; Renard, J. -P. *J. Phys. D: Appl. Phys.* **2003**, *36*, R127.
(14) de Teresa, J. M.; Barthélémy, A.; Contour, J. P.; Fert, A. *J. Magn. Magn. Mater.* **2000**, *211*, 160.
(15) Harada, T.; Ohkubo, I.; Lippmaa, M.; Sakurai, Y.; Matsumoto, Y.; Muto, S.; Koinuma, H.; Oshima, M. *Adv. Funct. Mater.* **2012**, *22*, 4471.
(16) Martin, C.; Maignan, A.; Hervieu, M.; Raveau, B. *Phys. Rev. B* **1999**, *60*, 12191.
(17) Kurbakov, A. I. *J. Magn. Magn. Mater.* **2010**, *322*, 967.
(18) Worledge, D. C.; Snyder, G. J.; Beasley, M. R.; Geballe, T. H.; Hiskes, R.; DiCarolis, S. *J. Appl. Phys.* **1996**, *80*, 5158.
(19) Prasad, R.; Singh, H. K.; Singh, M. P.; Prellier, W.; Siwach, P. K.; Kaur, A. *J. Appl. Phys.* **2008**, *103*, 083906.
(20) Salamon, M. B.; Jaime, M. *Rev. Mod. Phys.* **2001**, *73*, 583.
(21) Hassen, A.; Mandal, P. *J. Appl. Phys.* **2007**, *101*, 113917.
(22) Moodera, J. S.; Mathon, G. *J. Magn. Magn. Mater.* **1999**, *200*, 248.
(23) Santos, T. S.; Moodera, J. S.; Raman, K. V.; Negusse, E.; Holroyd, J.; Dvorak, J.; Liberati, M.; Idzerda, Y. U.; Arenholz, E. *Phys. Rev. Lett.* **2008**, *101*, 147201.
(24) Simmons, J. G. *J. Appl. Phys.* **1963**, *34*, 1793.
(25) Dalai, M. K.; Pal, P.; Sekhar, B. R.; Saini, N. L.; Singhal, R. K.; Garg, K. B.; Doyle, B.; Nannarone, S. *Phys. Rev. B* **2006**, *74*, 165119.
(26) LeClair, P.; Ha, J. K.; Swagten, H. J. M.; Kohlhepp, J. T.; van de Vin, C. H.; de Jonge, W. J. M. *Appl. Phys. Lett.* **2002**, *80*, 625.
(27) Harada, T.; Ohkubo, I.; Lippmaa, M.; Sakurai, Y.; Matsumoto, Y.; Muto, S.; Koinuma, H.; Oshima, M. *Phys. Rev. Lett.* **2012**, *109*, 076602.
(28) Mezei, F.; Zawadowski, A. *Phys. Rev. B* **1971**, *3*, 3127.
(29) LeClair, P.; Kohlhepp, J. T.; Swagten, H. J. M.; de Jonge, W. J. M. *Phys. Rev. Lett.* **2001**, *86*, 1066.
(30) Moodera, J. S.; Kinder, L. R. *J. Appl. Phys.* **1996**, *79*, 4724.
(31) Moodera, J. S.; Nowak, J.; van de Veerdonk, R. J. M. V. *Phys. Rev. Lett.* **1998**, *80*, 2941.
(32) Wolf, E. L. *Principle of Electron Tunneling Spectroscopy*, Oxford University Press, New York, 1985.
(33) Shen, L. Y. L.; Rowell, J. M. *Phys. Rev.* **1968**, *165*, 566.
(34) Rowell, J. M.; Shen, L. Y. L. *Phys. Rev. Lett.* **1966**, *17*, 15.
(35) Lee, K. I.; Joo, S. J.; Lee, J. H.; Rhie, K.; Kim, T. −S.; Lee, W. Y.; Shin, K. H.; Lee, B. C.; LeClair, P.; Lee, J. −S.; Park, J. −H. *Phys. Rev. Lett.* **2007**, *98*, 107202.
(36) Goldhaber-Gordon, D.; Göres, J.; Kastner, M. A. *Phys. Rev. Lett.* **1998**, *81*, 5225.
(37) Zhang, J.; Xu, Y.; Cao, S.; Cao, G.; Zhang, Y.; Jing, C. *Phys. Rev. B* **2005**, *72*, 054410.
(38) Kasai, M.; Kuwahara, H.; Tomioka, Y.; Tokura, Y. *J. Appl. Phys.* **1996**, *80*, 6894.
(39) Srivastava, M. K.; Singh, S.; Siwach, P. K.; Kaur, A.; Awana, V. P. S.; Maurya, K. K.; Singh, H. K. *AIP Adv.* **2013**, *3*, 052118.
(40) Bell, C.; Burnell, G.; Kang, D.-J.; Hadfield, R. H.; Kappers, M. J.; Blamire, M. G. *Nanotechnology* **2003**, *14*, 630.
(41) Wu, M. C.; Aziz, A.; Witt, J. D. S.; Hickey, M. C.; Ali, M.; Marrows, C. H.; Hickey, B. J.; Blamire, M. G. *Nanotechnology* **2008**, *19*, 485305.